



UNIVERSITY  
OF WOLLONGONG  
AUSTRALIA

University of Wollongong  
Research Online

---

Faculty of Engineering and Information Sciences -  
Papers: Part A

Faculty of Engineering and Information Sciences

---

2013

# Large networks of vertical multi-layer graphenes with morphology-tunable magnetoresistance

Zengji Yue

*University of Wollongong, zy709@uowmail.edu.au*

Igor Levchenko

*Csiro Materials Science And Engineering*

Shailesh Kumar

*Csiro, University of Sydney,*

Donghan Seo

*University Of Sydney*

Xiaolin Wang

*University of Wollongong, xiaolin@uow.edu.au*

*See next page for additional authors*

---

## Publication Details

Yue, Z., Levchenko, I., Kumar, S., Seo, D., Wang, X., Dou, S. and Ostrikov, K. Ken. (2013). Large networks of vertical multi-layer graphenes with morphology-tunable magnetoresistance. *Nanoscale*, 5 (19), 9283-9288.

Research Online is the open access institutional repository for the University of Wollongong. For further information contact the UOW Library: [research-pubs@uow.edu.au](mailto:research-pubs@uow.edu.au)

---

# Large networks of vertical multi-layer graphenes with morphology-tunable magnetoresistance

## Abstract

We report on the comparative study of magnetotransport properties of large-area vertical few-layer graphene networks with different morphologies, measured in a strong (up to 10 T) magnetic field over a wide temperature range. The petal-like and tree-like graphene networks grown by a plasma enhanced CVD process on a thin (500 nm) silicon oxide layer supported by a silicon wafer demonstrate a significant difference in the resistance-magnetic field dependencies at temperatures ranging from 2 to 200 K. This behaviour is explained in terms of the effect of electron scattering at ultra-long reactive edges and ultra-dense boundaries of the graphene nanowalls. Our results pave a way towards three-dimensional vertical graphene-based magnetoelectronic nanodevices with morphology-tuneable anisotropic magnetic properties.

## Keywords

networks, vertical, multi, layer, large, graphenes, magnetoresistance, morphology, tunable

## Disciplines

Engineering | Science and Technology Studies

## Publication Details

Yue, Z., Levchenko, I., Kumar, S., Seo, D., Wang, X., Dou, S. and Ostrikov, K. Ken. (2013). Large networks of vertical multi-layer graphenes with morphology-tunable magnetoresistance. *Nanoscale*, 5 (19), 9283-9288.

## Authors

Zengji Yue, Igor Levchenko, Shailesh Kumar, Donghan Seo, Xiaolin Wang, S X. Dou, and Kostya Ken Ostrikov

# Large networks of vertical multi-layer graphenes with morphology-tunable magnetoresistance†

Cite this: *Nanoscale*, 2013, 5, 9283

Zengji Yue,<sup>ab</sup> Igor Levchenko,<sup>bc</sup> Shailesh Kumar,<sup>bc</sup> Donghan Seo,<sup>cb</sup> Xiaolin Wang,<sup>a</sup> Shixue Dou<sup>a</sup> and Kostya (Ken) Ostrikov<sup>\*bac</sup>

We report on the comparative study of magnetotransport properties of large-area vertical few-layer graphene networks with different morphologies, measured in a strong (up to 10 T) magnetic field over a wide temperature range. The petal-like and tree-like graphene networks grown by a plasma enhanced CVD process on a thin (500 nm) silicon oxide layer supported by a silicon wafer demonstrate a significant difference in the resistance–magnetic field dependencies at temperatures ranging from 2 to 200 K. This behaviour is explained in terms of the effect of electron scattering at ultra-long reactive edges and ultra-dense boundaries of the graphene nanowalls. Our results pave a way towards three-dimensional vertical graphene-based magnetoelectronic nanodevices with morphology-tuneable anisotropic magnetic properties.

Received 31st January 2013

Accepted 26th March 2013

DOI: 10.1039/c3nr00550j

[www.rsc.org/nanoscale](http://www.rsc.org/nanoscale)

## 1 Introduction

Graphene, a 2D single sheet of graphite, shows extraordinarily high electron mobility, thermal conductivity and mechanical strength, and thus may be suitable for many applications such as nanoelectronics, spintronics and optoelectronics.<sup>1–3</sup> The unique magnetotransport properties of graphene, such as magnetoresistance (MR), are of a special interest due to the possible graphene application in various magnetoelectronic devices such as magnetic sensors.<sup>4–6</sup> Very large MR of a single-layer graphene has been theoretically predicted and experimentally observed in 1D graphene nanoribbons.<sup>7,8</sup>

The MR in 2D graphene could be positive and linear due to the Coulomb interaction.<sup>5,6</sup> It could also be negative due to quantum interference corrections to conductivity of 2D graphene.<sup>9,10</sup> A changeover from the negative to positive behaviour due to the transition from weak localization (WL) to weak antilocalization (WAL) in the high magnetic field was observed.<sup>11–13</sup> A large MR due to the tunnelling effect has also been observed in the nanocontact consisting of a Ni nanoprobe and carbon nanowalls. This effect may be very useful for sensing applications.<sup>14</sup> Quasi-periodic MR oscillations have been

observed in thick carbon nanowalls in a low magnetic field, but no theoretical analysis of this effect was provided.

However, until now no ways have been found to effectively control these unusual properties of 1D and 2D graphenes. The lack of such control significantly limits the application of graphenes in graphene-based nanodevices.

One possible way to enhance the level of control over the magnetotransport characteristics is to design three-dimensional (3D) graphene networks of various morphologies, where different configurations of graphene flakes (presence of edges, boundaries, connections between the flakes *etc.*) can be a factor modifying the properties of the whole network. Indeed, graphene morphology influences the motion and trajectories of carriers in a magnetic field (since the possible trajectories depend on the specific structure and morphology of the graphene), and hence, affects the classical magnetoresistance. Furthermore, the geometry of the graphene edges and boundaries affects the intervalley scattering and influences the weak localization and the enhancement of MR.

Three-dimensional networks consisting of vertically oriented few-layer graphene nanowalls can be an excellent platform for bio-sensors, energy storage devices, catalysts, electrodes for fuel cells and field emission displays.<sup>16–19</sup> However, synthesis of large graphene networks with highly controllable morphology is still a challenge. As a result, the morphology-dependent magneto-transport properties in large graphene networks have not yet been explored.

Here, we investigate the anisotropic magneto-transport properties in large three-dimensional few-layer graphene networks of two different (petal-like and tree-like) morphologies, grown by a highly controllable plasma-enabled process. We demonstrate that the magnetotransport in the networks

<sup>a</sup>Institute for Superconducting and Electronic Materials (ISEM), Faculty of Engineering, University of Wollongong, NSW 2522, Australia. E-mail: Xiaolin@uow.edu.au

<sup>b</sup>Plasma Nanoscience Centre Australia (PNCA), CSIRO Materials Science and Engineering, P. O. Box 218, Lindfield, NSW 2070, Australia

<sup>c</sup>Plasma Nanoscience, School of Physics, The University of Sydney, Sydney, NSW 2006, Australia. E-mail: Kostya.Ostrikov@csiro.au

† Electronic supplementary information (ESI) available: Fig. S1–S6, a schematic of the experimental setup, SEM and TEM characterizations, and details of electrical measurements. See DOI: 10.1039/c3nr00550j

with some unique features can be effectively controlled by the network microstructure and morphology. These results are promising for the development of next-generation morphology-tunable magnetoelectronic devices.

## 2 Experimental

Three-dimensional self-organized vertical graphene networks (VGNs) have been synthesized using a radio-frequency inductively coupled plasma-enhanced Chemical Vapour Deposition (CVD) technique. A schematic of the plasma-enhanced CVD (PECVD) reactor is shown in Fig. S1, ESI† The VGNs were grown on thick Si(100) substrates covered with a 500 nm  $\text{SO}_2$  layer. No catalysts and external substrate heating were used in this process.<sup>20–22</sup>

The growth process consisted of two stages. At the first stage, the substrates were processed in Ar plasma at the pressure of 2.5–3 Pa and discharge power of 700–800 W. During the treatment, substrates were negatively biased and heated by the plasma. At the second stage, graphene networks were grown in the plasma ignited in a mixture of  $\text{CH}_4$ ,  $\text{H}_2$ , and Ar gases at the same discharge power. The surface temperature (700 K) during the process was measured using a K-type thermocouple.

Depending on the substrate bias and gas mixture composition, different morphologies of the networks were produced. In this work we used a constant pressure and controlled the morphology by changing the gas composition, and specifically, by changing the relative percentage of hydrogen which strongly influences the growth processes due to the interaction with the growing graphene edges (see Table 1 for the specific process parameters used for the growth of petal-like and tree-like morphologies). As shown in this work, a dramatic change in the morphology can be observed when the hydrogen content is changed from 11 to 20%.

Importantly, the increased bias and process time used for the growth of the tree-like network resulted in the fragmentation of a silica layer and formation of  $\text{SiO}_2$  islands required for the formation of the tree-like network (in contrast to the smooth silica surface required for the formation of the petal-like structure).<sup>22</sup>

The four-probe magnetotransport measurements were performed in the temperature range between 2 and 300 K using a

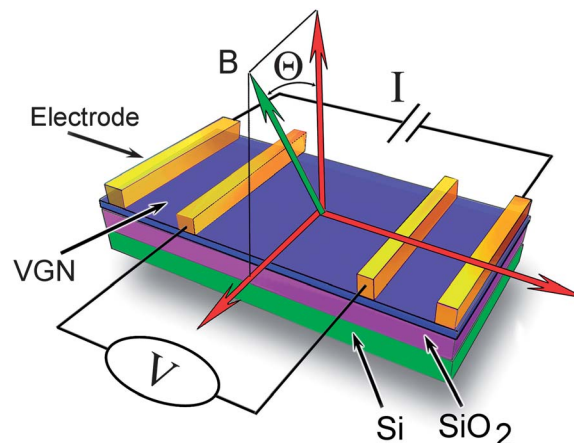


Fig. 1 Schematic of the magnetotransport measurements. The size of the sample is  $5 \text{ mm}^2$ .

14 T physical properties measurement system (PPMS). A schematic of the measurements is shown in Fig. 1. The area of the samples was  $5 \text{ mm}^2$ , and the distance between the two inner contacts was 1 mm. The resistances were obtained by applying a fixed electric current of  $10 \mu\text{A}$  through the two outer silver contacts and monitoring the voltage drop between the two inner contacts. The magnetic field  $B$  was applied along the vertical axis, perpendicular to the direction of the electric current. The MR was also measured by sweeping the magnetic field between 0 and 10 T. Rotation of the sample by  $360^\circ$  in a constant magnetic field was used to measure the anisotropic MR. The MR was calculated as  $(\rho_B - \rho_0/\rho_0) \times 100\%$ , where  $\rho_B$  and  $\rho_0$  are the resistivities with and without the magnetic field, respectively.

## 3 Results and discussion

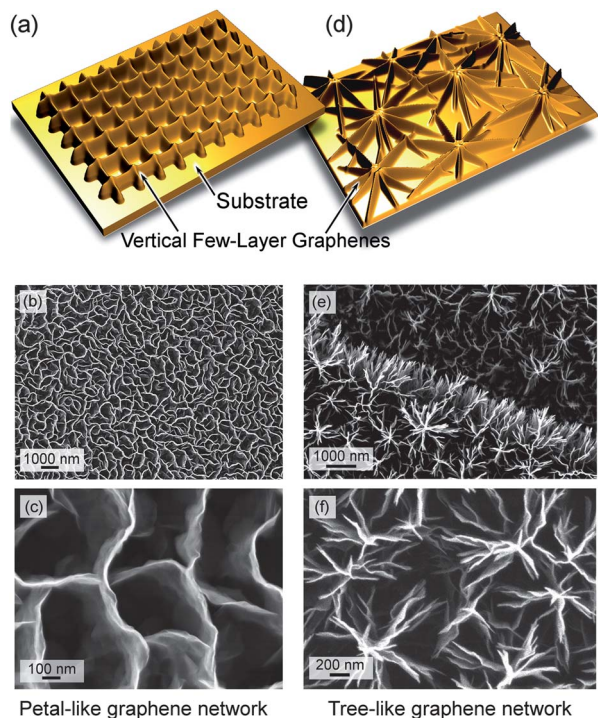
### Morphological and structural characteristics of the graphene networks

Fig. 2a–c show a schematic and scanning electron microscopy (SEM) images of the VGNs with petal-like morphology, in which graphene nanowalls are nearly perpendicular to the substrate, with the nanowall height ranging from 300 to 500 nm. Fig. 2d–f show the schematic and SEM images of the tree-like VGNs. As it can be seen, these two VGNs feature quite different structures. The petal-like network forms isolated cells of graphene nanowalls, whereas the tree-like network forms a branched structure. Importantly, the VGNs of the tree-like morphology have sharper boundaries and edges (Fig. 2f).

Fig. 3a–c show the low- and high-resolution TEM images, as well as a Raman spectrum of the vertical graphene nanowalls collected from the petal-like vertical graphene network (see also Fig. S2–S4, ESI†). From this image one can see that the petal-like morphology features ultra-long open reactive edges, which could serve as potential trapping sites of localized electrons. The TEM images and Raman spectrum of nanowalls collected from the tree-like network are shown in Fig. 3d and e. The high resolution TEM images confirm that the graphene nanowalls typically have only 3–7 layers. The distance between two

Table 1 Process parameters used for the growth of graphene networks of petal-like and tree-like morphologies

Morphology	Petal-like	Tree-like
$\text{SO}_2$ surface	Smooth	Islands
Substrate bias for Ar treatment, V	–50	–100
Time of Ar plasma treatment, min	3	10
Growth time, min	8	10
$\text{CH}_4$ content, %	30	44
$\text{H}_2$ content, %	20	11
Ar content, %	50	45
Thickness of graphene layers	3–5	5–7
Edge structure	Smooth	Sharp
Edge length, $\text{m g}^{-1}$	$10^5$	$10^7$



**Fig. 2** (a) Schematic and (b and c) low- and high-resolution SEM images of the petal-like graphene network. (d) Schematic and (e and f) low- and high-resolution SEM images of the tree-like graphene network. The petal-like network forms isolated cells, whereas the tree-like network forms a branched structure.

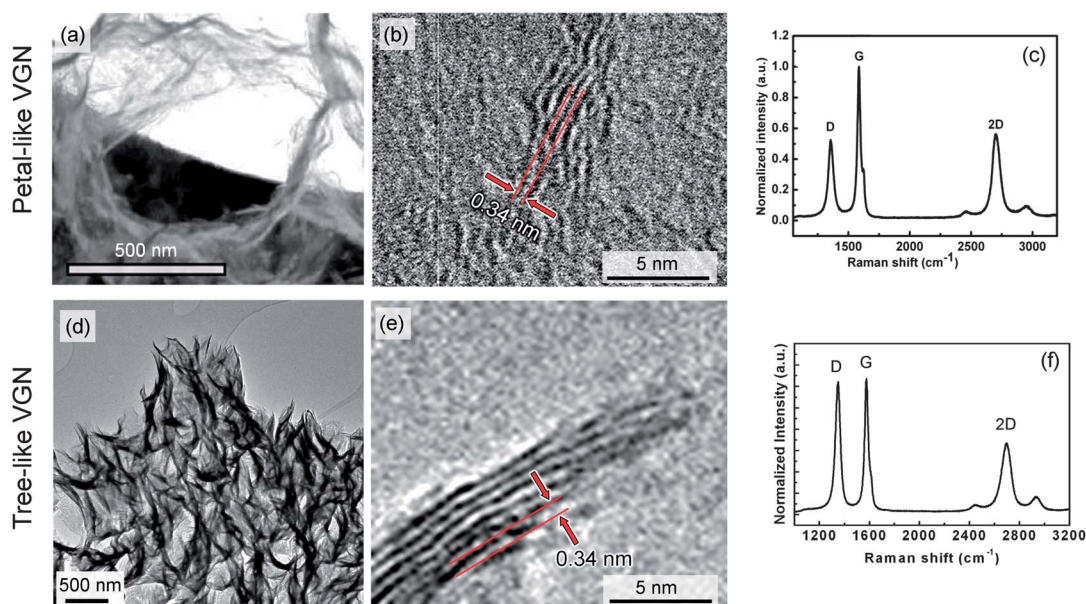
graphene layers is about 0.34 nm, as shown by the arrows. Raman spectra of the tree-like and petal-like networks contain a disorder-related D peak at  $1600\text{ cm}^{-1}$ , a graphitic G peak at  $1350\text{ cm}^{-1}$ , and a crystalline carbon-related 2D peak at  $2690\text{ cm}^{-1}$ , respectively. The relatively stronger D peak reveals that the

petal-like network has a lower order of graphitization and a higher density of defects. A more detailed comparison of the network parameters is shown in Table 1.

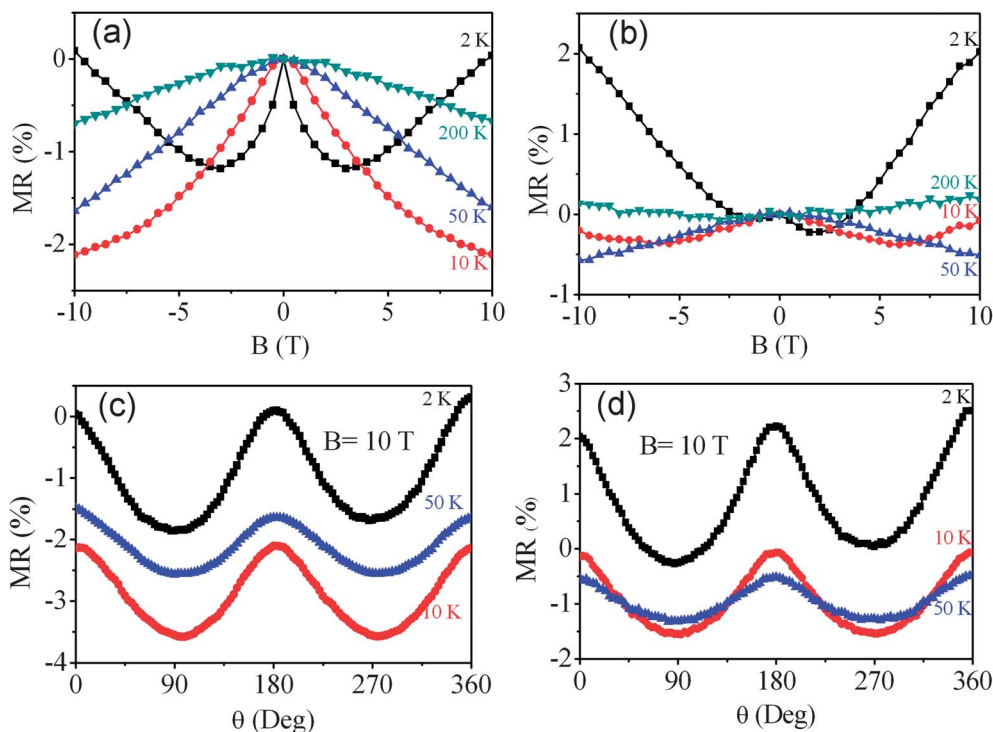
### Magnetotransport measurements

Fig. 4a and b show the MR measured on the petal-like and tree-like graphene networks with the temperature as a parameter and the magnetic field perpendicular to the sample surface. At lower magnetic fields, the MR always exhibits negative values and a quadratic field dependence, which can be fitted as  $\text{MR} = kB^2$ , where  $k$  is a constant. With the magnetic field increasing, the negative MR is strongly suppressed and a positive MR is observed. The MR has a sharp peak at  $B = 0$  at 2 K and a positive slope above 9.5 T. The magnetoresistance in both petal-like and tree-like structures displays strong temperature dependences. In petal-like networks, the absolute value of the magnetoresistance increases with decreasing temperature in weak magnetic fields ( $-3\text{ T} < B < 3\text{ T}$ ), but decreases sharply in strong magnetic fields ( $B < -3$  and  $B > 3\text{ T}$ ) at low (about 2 K) temperatures. On the other hand, the magnetoresistance in tree-like networks is relatively small at high temperatures ( $T > 50\text{ K}$ ) and increases to more than 2% at low (about 2 K) temperatures.

Compared with the large positive MR in the nanocontact consisting of ferromagnetic Ni and vertical carbon nanowalls, the observed MR in the petal-like graphene network can be attributed to the WL effects.<sup>14</sup> On the other hand, no MR oscillations have been observed in our samples, which might result from a morphology different from that of the thicker carbon nanowalls used in previous works.<sup>15</sup> The petal-like graphene network shows a relatively low order of graphitization with quite significant defects at ultralong edges and boundaries, where the electrons could be trapped and lead to localized states.



**Fig. 3** (a–c) Low- and high-resolution TEM images, and a Raman spectrum of vertical graphene nanowalls collected from the petal-like vertical graphene network. (d–f) Low- and high-resolution TEM images, and a Raman spectrum of vertical graphene nanowalls collected from the tree-like vertical graphene network.



**Fig. 4** (a and b) Magnetoresistance as a function of magnetic field at an angle  $\theta = 0$  in petal-like and tree-like graphene networks with the temperature as a parameter. (c and d) Angular dependencies of magnetoresistance in petal-like and tree-like VGNs with the temperature as a parameter.

Fig. 4c and d show angular dependencies of the MR for petal-like and tree-like graphene networks with temperature as a parameter. The MR in both types of networks shows a strong anisotropy with twofold symmetry over the whole temperature range. The maximum MR value appears at around  $0^\circ$  and  $180^\circ$  (*i.e.*, when the magnetic field is parallel to the side surfaces of the graphene nanowalls), and the minimum value is found at around  $90^\circ$  and  $270^\circ$  (with the magnetic field perpendicular to the side surfaces). Unlike the petal-like networks, the angular-dependent MR curves in the tree-like network display four intersections between 10 K and 50 K. More details on the magnetotransport measurements, as well as the resistance-temperature dependencies can be found in the ESI.†

### Interpretation of the anisotropic magnetoresistance

The anisotropic MR behaviour is usually observed in the ferromagnetic and non-magnetic materials due to a larger probability that electrons will experience s-d scattering in the direction of the magnetic field and due to anisotropy of the Fermi surface, respectively.<sup>29,30</sup> Anisotropic MR has also been observed in terraced graphene sheets and is attributed to geometric anisotropy.<sup>31,32</sup> The intervalley electron scattering leads to the observed enhancement of negative resistance and restoration of the weak localization in 2D graphene, whereas the antilocalization results from the suppressed intervalley scattering and chiral electronic character.<sup>23</sup>

The low-field magnetotransport in the 3D VGNs could be affected by various scattering mechanisms. Dense, ultra-long,

sharp and defect-prone edges might be the main sources of the intervalley scattering in our VGNs,<sup>6</sup> thus causing restoration of the weak localization (WL) and the observed enhancement of negative MR.

Importantly, the weak localization results from the quantum mechanical interference between elastically scattered carrier waves and occurs in phase-coherent conductors when there is constructive interference between two time-reversed electron paths.<sup>9</sup> The electron paths could be confined to the cavities of the graphene networks since the WL correction actually probes an area distribution of time-reversed paths.<sup>24</sup> Different directions of electron travel along a closed path induce an accumulation of the geometric phase, which contributes to the interference process.<sup>13</sup> The destruction of the WL by a weak magnetic field leads to a negative MR which is apparent in low magnetic fields.<sup>25</sup>

Besides, the magnetoresistance can be also affected by the ultra-long boundaries and vacancy defects on the surfaces of graphene nanosheets since the boundaries and surface defects can trap electrons and holes, and eventually lead to localized states and intervalley scattering. In our structures, the ultra-long edges are a mixture of zigzag and armchair types, both of which are highly defective. As shown clearly in the TEM images (Fig. 3), the edges of tree-like graphene networks are sharper than those of the petal-like networks, and this can result in a more pronounced effect on the intervalley scattering and magnetoresistance.

To analyze the obtained results, we will use the expression derived by McCann *et al.* for the MR associated with the weak localization in few-layer graphenes:<sup>26</sup>

$$\Delta\rho_B \equiv \rho_B - \rho_0 = -\frac{e^2\rho^2}{\pi h} \left[ F\left(\frac{B}{B_\phi}\right) - F\left(\frac{B}{B_\phi + 2B_i}\right) - 2F\left(\frac{B}{B_\phi + B_*}\right) \right], \quad (1)$$

where  $F(Z) = \ln Z + \psi\left(\frac{1}{2} + \frac{1}{Z}\right)$ ,  $B_{\phi,i,*} = \frac{\hbar c}{4De} \tau_{\phi,i,*}^{-1}$ . Here  $\psi$  is the digamma function,  $D$  is the diffusion coefficient,  $h$  is the Planck's constant, and  $\rho_B$  and  $\rho_0$  are the resistances in the presence of magnetic field and without magnetic field, respectively. When the isospin conservation scattering process dominates, the correction to the sheet MR can be expressed as:<sup>23</sup>

$$\Delta\rho_B = -\frac{e^2\rho^2}{\pi h} \left[ F\left(\frac{2\tau_\phi}{\tau_B}\right) - F\left(\frac{2}{\tau_B(\tau_\phi^{-1} + 2\tau_i^{-1})}\right) - 2F\left(\frac{2}{\tau_B(\tau_\phi^{-1} + \tau_i^{-1} + \tau_*^{-1})}\right) \right], \quad (2)$$

where  $\tau_B = \frac{\hbar}{2eDB}$ . Here,  $\tau_\phi$ ,  $\tau_i$ ,  $\tau_*$  are the phase coherence time, intervalley scattering time, and intravalley relaxation time, respectively.

Quantum interference correction to the MR in VGNs is dependent on the interplay of the intravalley and intervalley scattering. The first term in eqn (2) is responsible for WL, while the second and third terms with a negative sign lead to WAL. The MR is significantly affected by the competing relaxation mechanisms which occur in the graphene. This WL effect leads to the observation of a negative MR.

According to (2), the sign of WL in VGNs shows that the intervalley scattering time is shorter than the phase coherence time, *i.e.*,  $\tau_i < \tau_*$ . The WL-related MR could saturate at magnetic field strengths determined by the intervalley scattering time  $\tau_i$ . Such behaviour can be expected for our graphene networks which have ultra-long defective edges. Indeed, petal-like graphene networks display negative MR at low fields, thus confirming the theoretical predictions.

As can be seen in Fig. 4, tree-like networks also exhibit similar negative MR, with smaller values than the MR in the petal-like VGNs at low fields and high temperatures. However, the MR becomes positive even in a low field at a very low (2 K) temperature. Based on (1), the observed positive MR is a clear signature of WAL in tree-like VGNs. In this case, the WAL results from the suppression of backscattering because of the Berry phase, and suppression of WL due to the decreased intervalley scattering.<sup>26</sup> Interference corrections to the resistance appear with the decreased temperature since the elastic scattering becomes a dominant mechanism and inelastic scattering is strongly suppressed. This allows electrons to retain their phase coherence over long distances, and therefore the phase coherence time increases. Nevertheless, the WAL cannot exist at high temperatures owing to the strong phonon-electron scattering induced reduction of the phase coherence time  $\tau_\phi$ .<sup>11</sup>

Besides, spin-orbital interactions also can lead to WAL if graphene has broken the  $z \rightarrow z$  symmetry at the lowest temperatures.<sup>27</sup> The  $z \rightarrow z$  symmetry can be broken in tree-like VGNs with the nanoribbon-like sharp edges, and the spin-

orbital interaction is also stronger in the electron tunnelling process at the sharper boundaries. This will result in larger positive WAL-related MR at the lowest temperatures, which is consistent with our observations.

Therefore, the MR in VGNs can be tuned at low field and low temperature from WL in petal-like VGNs to WAL in tree-like VGNs through the edge design. In addition, the MR in the tree-like VGNs also demonstrates weak asymmetry, which has also been observed in hydrogenated graphene and can be attributed to the asymmetry in the electron-hole transport processes.<sup>28</sup>

Meanwhile, we stress that the network morphology is one of the possible features controlling the magnetoresistance. Other approaches influencing various physical processes involved in the origin of the magnetoresistance in graphene networks may be also efficient.

The charge carriers move through the entangled VGNs *via* distorted current paths misaligned with the bias direction.<sup>5</sup> In this case, the Lorentz forces induce curving of the electron trajectories and thus can result in a classical positive MR. Specifically, in a perpendicular magnetic field ( $\theta = 0^\circ/360^\circ, 180^\circ$ ) the carriers will be deflected in the plane of substrate surface, while they will be deflected out-of-plane in a parallel magnetic field ( $\theta = 90^\circ, 270^\circ$ ). However, the in-plane deflection of carrier trajectories is stronger than that of out-of-plane, which results in the MR anisotropy. The difference of the angular-dependent MR characteristics for the petal-like and tree-like VGNs results from a strong difference in the morphology of nanoarrays. This anisotropy of the MR could find application in designing VGN-based integrated angle sensors suitable for detecting the magnetic field polarity.

## 4 Conclusions

The anisotropic magnetotransport properties of the 3D vertical few-layer graphene networks have been investigated. We demonstrate effective tunability of the magnetotransport by controlling the morphology of self-organized three-dimensional graphene networks, which is quite challenging to obtain in 1D and 2D graphenes. Our results pave a way towards the 3D vertical graphene-based magnetoelectronic nanodevices with morphology-tuneable anisotropic properties.

## Acknowledgements

This work is partially supported by the Australian Research Council under Discovery Project DP1094073 and Future Fellowship Project FT100100303. Z.Y. thanks CSIRO for an OCE PhD top-up fellowship.

## References

- 1 A. H. Castro Neto, F. Guinea, N. M. R. Peres, K. S. Novoselov and A. K. Geim, *Rev. Mod. Phys.*, 2009, **81**, 109–162.
- 2 F. Shen, D. Wang, R. Liu, X. Pei, T. Zhang and J. Jin, *Nanoscale*, 2013, **5**, 537–540.
- 3 R. S. Edwards and K. S. Coleman, *Nanoscale*, 2013, **5**, 38–51.

- 4 J.-H. Chen, L. Li, W. G. Cullen, E. D. Williams and M. S. Fuhrer, *Nat. Phys.*, 2011, **7**, 535–538.
- 5 Z.-M. Liao, H.-C. Wu, S. Kumar, G. S. Duesberg, Y.-B. Zhou, G. L. W. Cross, I. V. Shvets and D.-P. Yu, *Adv. Mater.*, 2012, **24**, 1862–1866.
- 6 A. L. Friedman, J. L. Tedesco, P. M. Campbell, J. C. Culbertson, E. Aifer, F. K. Perkins, R. L. Myers-Ward, J. K. Hite, C. R. Eddy, G. G. Jernigan and D. K. Gaskill, *Nano Lett.*, 2010, **10**, 3962–3965.
- 7 W. Y. Kim and K. S. Kim, *Nat. Nanotechnol.*, 2008, **3**, 408–412.
- 8 J. Bai, R. Cheng, F. Xiu, L. Liao, M. Wang, A. Shailos, K. L. Wang, Y. Huang and X. Duan, *Nat. Nanotechnol.*, 2010, **5**, 655–659.
- 9 F. V. Tikhonenko, D. W. Horsell, R. V. Gorbachev and A. K. Savchenko, *Phys. Rev. Lett.*, 2008, **100**, 056802.
- 10 D.-K. Ki, D. Jeong, J.-H. Choi, H.-J. Lee and K.-S. Park, *Phys. Rev. B: Condens. Matter Mater. Phys.*, 2008, **78**, 125409.
- 11 F. V. Tikhonenko, A. A. Kozikov, A. K. Savchenko and R. V. Gorbachev, *Phys. Rev. Lett.*, 2009, **103**, 226801.
- 12 S. Pezzini, C. Cobaleda, E. Diez and V. Bellani, *Phys. Rev. B: Condens. Matter Mater. Phys.*, 2012, **85**, 165451.
- 13 Y. Liu, W. S. Lew and L. Sun, *Phys. Chem. Chem. Phys.*, 2011, **13**, 20208–20214.
- 14 C. Zhang, Y. Wang, L. Huang and Y. Wu, *Appl. Phys. Lett.*, 2010, **97**, 062102.
- 15 Y. Wu, B. Yang, B. Zong, H. Sun, Z. Shen and Y. Feng, *J. Mater. Chem.*, 2004, **14**, 469–477.
- 16 H. Terrones, R. Lv, M. Terrones and M. S. Dresselhaus, *Rep. Prog. Phys.*, 2012, **75**, 062501.
- 17 D. Pan, S. Wang, B. Zhao, M. Wu, H. Zhang, Y. Wang and Z. Jiao, *Chem. Mater.*, 2009, **21**, 3136–3142.
- 18 N. G. Shang, P. Papakonstantinou, M. McMullan, M. Chu, A. Stamboulis, A. Potenza, S. S. Dhesi and H. Marchetto, *Adv. Funct. Mater.*, 2008, **18**, 3506–3514.
- 19 X. Xiao, P. Liu, J. S. Wang, M. W. Verbrugge and M. P. Balogh, *Electrochem. Commun.*, 2011, **13**, 209–212.
- 20 K. Ostrikov, *Rev. Mod. Phys.*, 2005, **77**, 489–511.
- 21 D. H. Seo, S. Kumar and K. Ostrikov, *J. Mater. Chem.*, 2011, **21**, 16339–16343.
- 22 S. Kumar and K. Ostrikov, *Nanoscale*, 2011, **3**, 4296–4300.
- 23 X. Wu, X. Li, Z. Song, C. Berger and W. A. de Heer, *Phys. Rev. Lett.*, 2007, **98**, 136801.
- 24 J. Eroms and D. Weiss, *New J. Phys.*, 2009, **11**, 095021.
- 25 S. N. Song, X. K. Wang, R. P. H. Chang and J. B. Ketterson, *Phys. Rev. Lett.*, 1994, **72**, 697–700.
- 26 E. McCann, K. Kechedzhi, V. I. Fal'ko, H. Suzuura, T. Ando and B. L. Altshuler, *Phys. Rev. Lett.*, 2006, **97**, 146805.
- 27 E. McCann and V. I. Fal'ko, *Phys. Rev. Lett.*, 2012, **108**, 166606.
- 28 B. R. Matis, F. A. Bulat, A. L. Friedman, B. H. Houston and J. W. Baldwin, *Phys. Rev. B: Condens. Matter Mater. Phys.*, 2012, **85**, 195437.
- 29 P. Wisniewski, *Appl. Phys. Lett.*, 2007, **90**, 192106.
- 30 Z. Zhu, A. Collaudin, B. Fauque, W. Kang and K. Behnia, *Nat. Phys.*, 2012, **8**, 89–94.
- 31 M. K. Yakes, D. Gunlycke, J. L. Tedesco, P. M. Campbell, R. L. Myers-Ward, C. R. Eddy, D. K. Gaskill, P. E. Sheehan and A. R. Laracuente, *Nano Lett.*, 2010, **10**, 1559–1562.
- 32 B. Jouault, B. Jabakhanji, N. Camara, W. Desrat, A. Tiberj, J. R. Huntzinger, C. Consejo, A. Caboni, P. Godignon, Y. Kopelevich and J. Camassel, *Phys. Rev. B: Condens. Matter Mater. Phys.*, 2010, **82**, 085438.